RESEARCH ARTICLE

Key Points:
- Cloud cover and mixed-phase parameterizations have compensating effects on planetary albedo in GCMs.
- Models that maintain liquid to lower temperatures have less cloud cover.
- This compensation affects both the climate mean-state and cloud feedback.

Correspondence to:
D. T. McCoy,
dtmccoy@atmos.uw.edu

On the relationships among cloud cover, mixed-phase partitioning, and planetary albedo in GCMs

Daniel T. McCoy[1], Ivy Tan[2], Dennis L. Hartmann[1], Mark D. Zelinka[3], and Trude Storelvmo[2]

[1]Atmospheric Sciences Department, University of Washington, Seattle, Washington, USA, [2]Geology and Geophysics Department, Yale University, New Haven, Connecticut, USA, [3]Program for Climate Model Diagnosis and Intercomparison, Lawrence Livermore National Laboratory, Livermore, California, USA

Abstract In this study, it is shown that CMIP5 global climate models (GCMs) that convert supercooled water to ice at relatively warm temperatures tend to have a greater mean-state cloud fraction and more negative cloud feedback in the middle and high latitude Southern Hemisphere. We investigate possible reasons for these relationships by analyzing the mixed-phase parameterizations in 26 GCMs. The atmospheric temperature where ice and liquid are equally prevalent (T5050) is used to characterize the mixed-phase parameterization in each GCM. Liquid clouds have a higher albedo than ice clouds, so, all else being equal, models with more supercooled liquid water would also have a higher planetary albedo. The lower cloud fraction in these models compensates the higher cloud reflectivity and results in clouds that reflect short-wave radiation (SW) in reasonable agreement with observations, but gives clouds that are too bright and too few. The temperature at which supercooled liquid can remain unfrozen is strongly anti-correlated with cloud fraction in the climate mean state across the model ensemble, but we know of no robust physical mechanism to explain this behavior, especially because this anti-correlation extends through the subtropics. A set of perturbed physics simulations with the Community Atmospheric Model Version 4 (CAM4) shows that, if its temperature-dependent phase partitioning is varied and the critical relative humidity for cloud formation in each model run is also tuned to bring reflected SW into agreement with observations, then cloud fraction increases and liquid water path (LWP) decreases with T5050, as in the CMIP5 ensemble.

1. Introduction

The low cloud response to warming remains one of the largest sources of uncertainty in the representation of the overall climate feedback [*Bony et al.*, 2006; *Dufresne and Bony*, 2008; *Vial et al.*, 2013; *Webb et al.*, 2013; *Zelinka et al.*, 2012, 2013]. It is important to note that not only the change in the clouds with warming relative to the control climate, but the control climate itself also modulates climate feedbacks in models [*Grise et al.*, 2015; *Trenberth and Fasullo*, 2010].

Recent studies have identified several robust features of the GCM-simulated low cloud feedback. In the subtropics, low cloud cover decreases with warming, leading to a positive feedback [*Brient and Bony*, 2013; *Qu et al.*, 2014, 2015; *Zelinka et al.*, 2012, 2013]. While observations and cloud resolving models agree qualitatively with GCMs in predicting a decrease in cloud cover with rising SSTs, no strong consensus as to the mechanisms that lead to this decrease has emerged, and it is not clear how well the critical mechanisms are treated in GCMs [*Blossey et al.*, 2013; *Bretherton and Blossey*, 2014; *Bretherton et al.*, 2013; *Brient et al.*, 2015; *Clement et al.*, 2009; *Klein et al.*, 1995; *Myers and Norris*, 2013, 2014; *Norris and Leovy*, 1994; *Qu et al.*, 2014, 2015]. In midlatitudes the cloud feedback becomes robustly negative as cloud optical depth increases in step with warming [*Zelinka et al.*, 2012, 2013]. The increase in cloud optical depth with warming in this region has been attributed to transitions from relatively unreflective ice to relatively bright liquid condensate [*Ceppi et al.*, 2015; *Choi et al.*, 2014; *Gordon and Klein*, 2014; *Komurcu et al.*, 2014; *McCoy et al.*, 2014b, 2015a; *Naud et al.*, 2006; *Tsushima et al.*, 2006; *Zelinka et al.*, 2012, 2013].

The treatment of mixed-phase clouds in GCMs is highly uncertain. *McCoy et al.* [2015a] showed that 19 GCMs from the Coupled Model Intercomparison Project phase 5 (CMIP5) effectively partition ice and liquid as a monotonic function of atmospheric temperature, even though some of the GCMs include prognostic mixed-phase cloud physics [*Cesana et al.*, 2015; *Komurcu et al.*, 2014]. Monotonic partitioning of ice and

liquid as a function of temperature was also demonstrated by *Cesana et al*. [2015] for a different set of GCMs. *McCoy et al*. [2015a] demonstrated that the temperature where ice and liquid were diagnosed to be equally prevalent (T5050) in the GCMs varied by up to 35 K in the 19 models surveyed. Across-model variations in T5050 were shown to determine a substantial fraction of the across-model variations in LWP increases between the control climate and the RCP8.5 scenario in the Southern Ocean region. While disquieting from the perspective of constraining climate uncertainty, this is not inconsistent with the complexity of the processes that take place in mixed-phase clouds. Ice and liquid have very different microphysical and radiative properties. Transitions between the two states as dictated by nucleation, secondary ice formation, and the Bergeron-Findeisen process remain poorly constrained observationally and in large-eddy simulations [*Atkinson et al*., 2013; *Cesana et al*., 2015; *Kanitz et al*., 2011; *Komurcu*, 2015; *Komurcu et al*., 2014; *Korolev et al*., 2003; *Morrison et al*., 2011; *Murray et al*., 2012].

Because of this lack of robust constraint on the processes that take place in mixed-phase clouds, GCMs portray these processes in a wide variety of ways [*Cesana et al*., 2015; *Komurcu et al*., 2014; *McCoy et al*., 2015a]. As has been shown, the partitioning of ice and liquid in mixed-phase clouds exerts a strong control on cloud albedo [*McCoy et al*., 2014a,b]. This allows the uncertainties in the mixed-phase parameterization of a given model to strongly affect both the SW radiation that is reflected in the climate mean-state and the change in reflected SW radiation with warming.

In section 2, we discuss the model data used in this study, the derivation of each model's T5050 parameter, and the observational data sets used to evaluate model behavior. In section 3, we discuss the across-model dependence of the climate mean state on each model's mixed-phase parameterization. We also discuss how adjustments of climate models that are needed to make the resulting cloud radiative effects agree with observations may depend on how the mixed phase processes are parameterized. A set of perturbed physics runs in CAM4 is used to support these results. Finally, we discuss how across-model variations in mixed-phase parameterizations affect cloud feedback.

2. Methods

GCMs have been shown to effectively partition ice and liquid in a given atmospheric volume as a monotonic function of atmospheric temperature, even if the GCM does not use a simple function of temperature to determine partitioning [*Cesana et al*., 2015; *McCoy et al*., 2015a]. We can characterize the curve of liquid to total condensate for each GCM in terms of the temperature where ice and liquid are equally prevalent, referred to as T5050. It should be noted that this characterization is relatively crude. Two GCMs can have very different curves describing their phase partitioning, but the same T5050. The midpoint of the curve describes the general position of the curve and provides a rough estimate of the temperatures at which supercooled liquid exists for a given model. Using the same techniques as *McCoy et al*. [2015a], we calculate T5050 for 26 GCMs from the CMIP5 archive at monthly mean temporal resolution using the latitude band from 30°S to 70°S (Figure 1a). Liquid and ice cloud water content are used to calculate the fraction of liquid to total water in the monthly mean data from 1850 to 1900 resolved at the native vertical and horizontal resolution of each model. This is composited on atmospheric temperature for each grid cell and a curve describing the fraction of liquid water as a function of atmospheric temperature is created. This yields 26 T5050s, one to describe each of the 26 GCMs (Table 1). Because the partitioning curves shown in Figure 1 are created using monthly mean data they are not equivalent to the curves that some of the models use to partition ice and liquid when condensate forms.

The 30°S–70°S latitude band in the Southern Ocean was chosen because it offers a large amount of data describing low, mixed-phase clouds and will be used to calculate T5050 for the remainder of this paper. It should be noted that while we might expect the Northern Hemisphere clouds to be more glaciated than the Southern Hemisphere clouds due to a higher loading of continental dust [*Atkinson et al*., 2013; *Kanitz et al*., 2011; *Tan et al*., 2014], the T5050 from GCMs does not appear to change drastically between the Northern and Southern Hemisphere oceans (Figure 1b). A few models do appear to have a Northern Hemisphere T5050 that is a few kelvin higher than the Southern Hemisphere, but the majority have the same T5050 in both hemispheres (Table 1). The same T5050 in the Northern and Southern Hemispheres contradicts observations from surface lidar and CALIPSO [*Hu et al*., 2010; *Kanitz et al*., 2011; *Tan et al*., 2014].
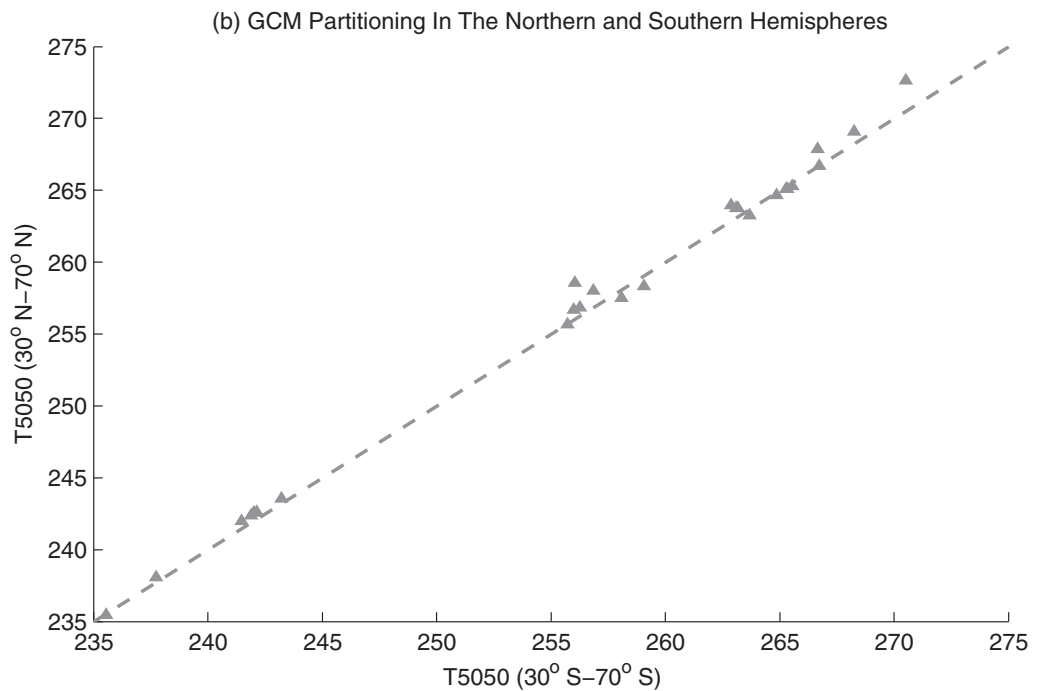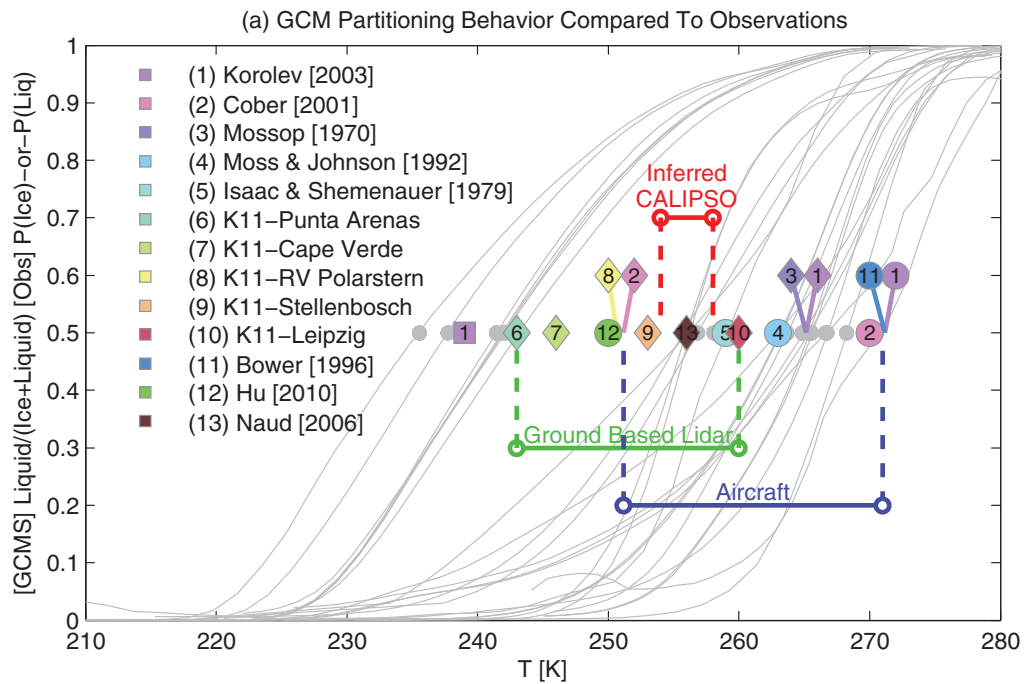
Figure 1. Comparison of GCM and observed water partitioning behaviors. (a) Grey curves show the fraction of liquid as a function of temperature in the 26 GCMs examined in this study. Data describing liquid and ice partitioning are gathered over oceans between 30°S and 70°S. The temperature where ice and liquid are equally common (T5050) for each model is shown using a grey circle and listed in Table 1. Colored markers are used to denote previous observational estimates of T5050 derived from the probability of observing ice or liquid cloud as a function of temperature. If the T5050 is derived from an instrument that measures the probability of detecting liquid clouds a circle is used, if it measures the probability of detecting ice clouds a diamond is used. Data points that are close together are shifted for visual clarity with a line indicating their true position. The ice probability from *Korolev et al.* [2003] is corrected for bouncing of ice particles [*Storelvmo et al.*, 2015], and the original data are shown as a square. It should be noted that the mass phase ratio from the GCMs and the probability of ice or liquid detection are not completely analogous quantities (see text and Figure 2). (b) the T5050 calculated using GCM data taken from Northern Hemisphere oceans (30°N–70°N) are compared to the T5050 calculated using GCM data taken from the Southern Hemisphere oceans (30°S–70°S). The one-to-one line is shown using grey dashes.

Table 1. List of Models Used in This Study[a]

| Model	T5050 (K) (30°S–70°S)	ΔT5050 (K) (MMM)	T5050 (K) (30°N–70°N)	ΔT5050 (K) (MMM)
CESM1-BGC	235.6	−20.9	235.4	−21.5
BNU-ESM	237.7	−18.8	238.1	−18.8
CCSM4	241.5	−15	242	−14.9
bcc-csm1-1	241.9	−14.6	242.4	−14.5
NorESM1-ME	242	−14.5	242.6	−14.3
NorESM1-M	242.1	−14.4	242.6	−14.3
bcc-csm1-1-m	243.2	−13.3	243.5	−13.4
CALIPSO (lower bound)	254.0	−2.5		
inmcm4	255.7	−0.8	255.7	−1.2
MRI-CGCM3	256	−0.5	258.6	1.7
GISS-E2-R	256	−0.5	256.7	−0.2
GISS-E2-H	256.3	−0.2	256.9	0
CNRM-CM5	256.8	0.3	258	1.1
CALIPSO (upper bound)	258.0	1.5		
CanESM2	258.1	1.6	257.5	0.6
CESM1-CAM5	259.1	2.6	258.3	1.4
GFDL-CM3	262.9	6.4	263.9	7
MIROC-ESM-CHEM	263.1	6.6	263.8	6.9
MIROC-ESM	263.2	6.7	263.8	6.9
IPSL-CM5B-LR	263.7	7.2	263.3	6.4
GFDL-ESM2G	264.9	8.4	264.7	7.8
IPSL-CM5A-LR	265.3	8.8	265.1	8.2
GFDL-ESM2M	265.3	8.8	265.1	8.2
IPSL-CM5A-MR	265.6	9.1	265.3	8.4
MIROC5	266.7	10.2	267.9	11
MPI-ESM-LR	266.7	10.2	266.7	9.8
CSIRO-Mk3-6-0	268.2	11.7	269.1	12.2
FGOALS-g2	270.5	14	272.6	15.7

[a]The Northern and Southern Hemisphere T5050 are listed by each model. Models are sorted by Southern Hemisphere T5050. The difference of each model's T5050 relative to the multimodel mean is noted as ΔT5050 (MMM). The multimodel mean is calculated separately in each hemisphere. The upper and lower bounds of the estimated range of T5050 from CALIPSO are shown for comparison (Figure 2). Note that the Southern Ocean T5050 is used to infer the range of T5050 from CALIPSO.

The probability of observing either ice or liquid clouds as a function of temperature derived from aircraft data and surface-based lidar is shown for comparison to the model diagnosed T5050s [*Bower et al.*, 1996; *Cober et al.*, 2001; *Isaac and Schemenauer*, 1979; *Kanitz et al.*, 2011; *Korolev et al.*, 2003; *Moss and Johnson*, 1994; *Mossop et al.*, 1970]. Data from *Korolev et al.* [2003] were revised as discussed in *Storelvmo et al.* [2015] to account for large ice particles shattering upon entering the inlets of cloud particle probes. Similar artifacts are likely to exist in the other aircraft data sets we present, and the aircraft data presented in Figure 1 are intended to show the range of observational estimates of mixed-phase behavior that exist in the literature. Both the revised and original aircraft data are shown. The aircraft data are measured in a variety of geographic regions and cloud regimes and span a temperature range that is almost as large as the models (Figure 1a). Surface-based lidar data from *Kanitz et al.* [2011] describing the probability of observing ice cloud is shown for a variety of polluted and pristine aerosol regimes. *Naud et al.* [2006] used data from the MODIS instrument to measure the fraction of ice clouds to all cloud detections in midlatitude storms in the wintertime Pacific and Atlantic. *Hu et al.* [2010] used a global data set from the Cloud-Aerosol Lidar and Infrared Pathfinder Satellite Observation (CALIPSO) satellite to describe the probability of detecting liquid cloud near cloud top.

It should be noted that the T5050 parameter described in *McCoy et al.* [2015a] is based on GCM liquid and ice mass output, while the phase ratio described in *Hu et al.* [2010] is measured by the cloud lidar near cloud top. As discussed in *Cesana et al.* [2015], these are not directly comparable, except when ice is 90% of the mass. When the water is 10% liquid and 90% ice (T1090) the simulated CALIPSO phase fraction and GCM mass phase fraction are relatively similar. To estimate the mass phase fraction implied by CALIPSO measurements we fit each model's T5050–T1090. The value of $T1090_{CALIPSO}$ is taken to be 243.15K. It is important to note that while the $T1090_{CALIPSO}$ differs very little between the SO and global ocean, systematic errors cannot be fully evaluated in the CALIPSO data [*Hu et al.*, 2010]. The T5050 consistent with $T1090_{CALIPSO}$ was predicted using 10,000 bootstrap samples. The value of T5050 that would be consistent with CALIPSO is predicted to be between 254 K and 258 K in 95% of the bootstrap samples (Figures 1a and 2). While imperfect, the fit of the GCM T1090 to T5050 at least gives a crude estimate of how the CALIPSO derived T5050 might map to the mass ratio derived T5050. Similarly, we might expect the phase ratios measured by aircraft, surface-based lidar, and passive remote sensing from MODIS to not directly compare to the GCM mass phase ratio.

For the remainder of this study we will compare the GCM diagnosed T5050 to the CALIPSO inferred T5050. The derivation of CALIPSO T5050 is imperfect, but it is the only data set that has not been subset to a specific cloud type or geographic region. We present the historical in-situ estimates of T5050 in Figure 1a to offer insight into some of the potential origins of the spread in GCM parameterizations. T5050s diagnosed
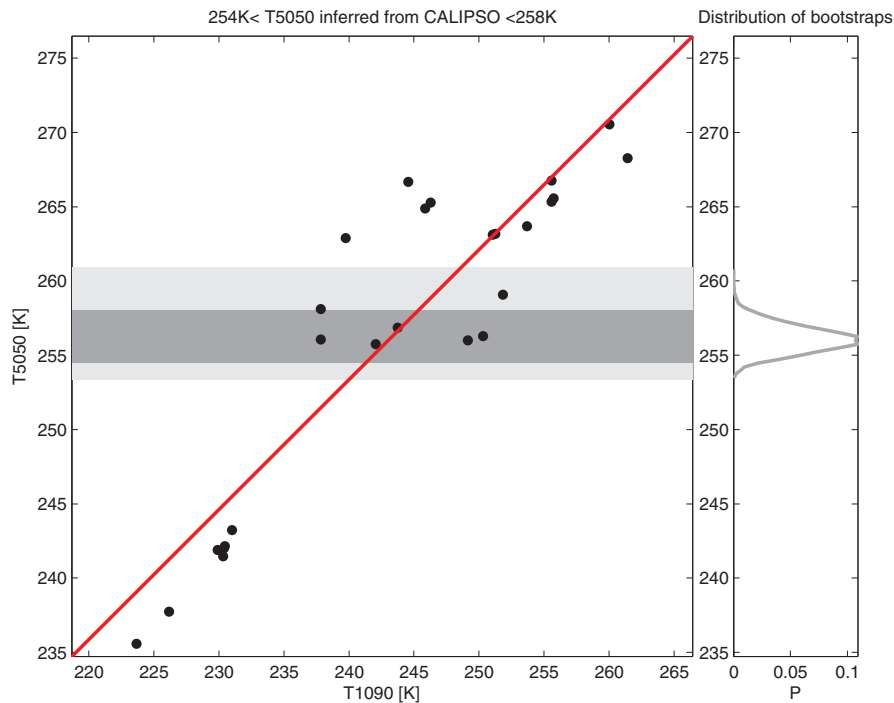
Figure 2. T5050 versus T1090 (10% liquid, 90% ice) for 26 GCMs. The observational value of T1090 from CALIPSO is used to predict the value of T5050 using 10,000 bootstrap samples. The distribution of T5050s calculated from the bootstrap samples is shown on the right. Light shading is used to show the minimum and maximum T5050 values inferred by the bootstraps and dark shading is used to show the range that 95% of the bootstrap estimates inhabit. The 95% confidence range of T5050 predicted from T1090 is 254K to 258K as noted in the title.

from *Kanitz et al.* [2011] and *Naud et al.* [2006] incorporate larger volumes of data and are less restricted by cloud type or geographic region. The results from these studies seem to cluster around the global estimate inferred by the CALIPSO instrument [*Hu et al.*, 2010]. Evidently the range in T5050 inferred from these studies assuming that phase-ratio is predictive of mass-ratio is still uncertain (243K in pristine clouds near Punta Arenas, Chile to 260K in continental measurements from Leipzig, Germany). Even though the surface-based observational range of mixed-phase behaviors is wide, 18 out of 26 of the T5050s did not fall in the range indicated by these measurements. Six had T5050s that were lower than the most pristine lidar measurements (243K). The remaining twelve models had T5050s that were higher than the T5050 measured over the continental European site (260K).

In addition to the T5050, we use the liquid water path (LWP), total cloud fraction (CF), upwelling SW, skin temperature, and pressure velocity at 500hPa. These are retrieved for the period 1850–1900 in the historical emissions scenario for each of the GCMs. GCM data from the RCP8.5 emissions scenario from the period 2025–2075 are used to compare the climate mean-state to a warmed climate. In-cloud LWP is estimated as the LWP divided by CF. This estimate is very crude and is only intended to help disentangle the covariance between LWP and CF, rather than serve as a rigorous estimate of the in-cloud LWP. Monthly climatologies are created on a 2.5° × 2.5° latitude-longitude grid for each model. The SW cloud feedback for each model is calculated as the temperature-mediated response of cloud-induced shortwave radiation anomalies in abrupt 4xCO2 simulations using the approximate partial radiative perturbation (APRP) method of *Taylor et al.* [2007].

In this study we focus on the effect of the mixed-phase parameterization on SW cloud reflectivity. Several clear a-priori reasons suggest that mixed-phase partitioning should affect the reflected SW, and models show a large spread in SW low-cloud feedbacks in the Southern Ocean [*Zelinka et al.*, 2012, 2013]. The effect of the mixed-phase cloud parameterization on the reflected SW can occur through several microphysical pathways: ice particles tend to be larger and less reflective than liquid [*Heymsfield et al.*, 2003; *McCoy et al.*, 2014a]; ice tends to precipitate more easily than liquid and depletes the cloud water more rapidly [*McCoy*

et al., 2015a; *Morrison et al.*, 2011]; and ice precipitation can also thin clouds and decrease cloud fraction [*Heymsfield et al.*, 2009; *Morrison et al.*, 2011]. The effects of the mixed-phase parameterization on cloud longwave (LW) radiative properties are less clear and LW cloud feedback seems to be less important in the Southern Ocean [*Zelinka et al.*, 2012, 2013].

Cloud parameterizations are complex and it is difficult to isolate a particular factor that controls inter-model behavior. To determine whether the diagnosed CMIP5 behaviors are consistent with compensation between mixed-phase behavior and cloud cover in each GCM, we compare our analysis to an ensemble of CAM4 simulations where the cloud physics have been systematically perturbed.

The observations of cloud properties used in this study are provided by the Moderate Resolution Imaging Spectroradiometer (MODIS) instrument collection 5.1 data set [*Platnick et al.*, 2003]; and the unified microwave liquid water path data set described in *O'Dell et al.* [2008] (UWISC). Uncertainty in cloud cover was estimated by contrasting the cloud mask and the cloud fraction excluding partially cloudy pixels. The difference between these quantities is especially large in broken cloud scenes [*Marchand et al.*, 2010]. The range of the in-cloud LWP was estimated using the MODIS retrieval and the UWISC microwave LWP divided by the MODIS cloud mask.

3. Results

3.1. Effects of Mixed-Phase Parameterization on Climate Mean-State

As shown over the Southern Ocean in *McCoy et al.* [2015a], T5050 is strongly negatively correlated with mean-state cloud liquid mass and strongly positively correlated with mean-state cloud ice mass. LWP strongly affects albedo, indicating that T5050 is likely to affect reflected SW. To examine the control of upwelling SW exerted by the model mixed-phase parameterization we regress annual mean upwelling SW on T5050 across-models at each latitude and longitude (Figure 3). Significant ($p<0.05$) negative correlations occur over the high-latitude oceans and in regions of large-scale ascent near the equator. Low-topped, mixed-phase clouds are prevalent in high latitudes and convective clouds that contain substantial ice and liquid are prevalent in the convective tropics. The sign of the correlation with SW is consistent with the idea that models that more readily create ice contain less liquid and are therefore less reflective.

Large, robust positive correlations between upwelling SW and T5050 exist across the subtropics indicating that models that do not maintain supercooled liquid at colder temperatures also reflect more SW in the subtropics. This is surprising because supercooled liquid clouds are uncommon in the subtropics. Even if supercooled liquid clouds were common in the subtropics, we would not expect this behavior based on the argument that models that create ice more readily have a lower LWP and therefore a lower albedo. The slope of the linear regression of upwelling SW on T5050 can be quite substantial in the midlatitudes and subtropics. Sensitivities can reach 1 W/m^2 for a 1 degree change in T5050 (Figure 3), or 10 W/m^2 per standard deviation in T5050 across the GCMs considered in this study. To understand the relationship between T5050 and SW we will examine the behavior of various cloud properties across GCMs in relation to their mixed-phase parameterizations.

In nearly every location, models with higher T5050 have larger CF and smaller LWP and CF-normalized LWP (Figure 4). It is interesting to note that the correlation between T5050 and upwelling SW is zero near 50°S (Figure 3) as the control of upwelling SW by T5050 transitions from being moderated by cloud fraction in the subtropics to cloud liquid water path in the midlatitudes (Figure 4). The relation between T5050 and cloud fraction and liquid water path is weaker in the tropics. The mean-state general circulation differs substantially between models, making the comparison of cloud properties in the convective tropics problematic. In order to compare differences in cloud properties between similar regimes we composite each cloud property on large-scale subsidence, in keeping with previous studies [*Bony et al.*, 2004]. We examine the correlation between cloud properties and T5050 as a function of large-scale vertical motion at 500 hPa over oceans. Equal quantiles of subsidence are created for the GCMs and the regression of GCM cloud properties on T5050 is performed in each quantile. LWP and the cloud-fraction-normalized LWP correlate negatively with T5050 across all vertical velocity bins (Figure 5). This correlation is significant at 95% confidence at pressure velocities less than 1.5 hPa/s. The cloud fraction is significantly correlated with T5050 across all pressure velocity regimes. The sign of this correlation is in contradiction to observations of supercooled liquid clouds, which show that enhanced glaciation (i.e., larger T5050) tends to decrease cloud fraction
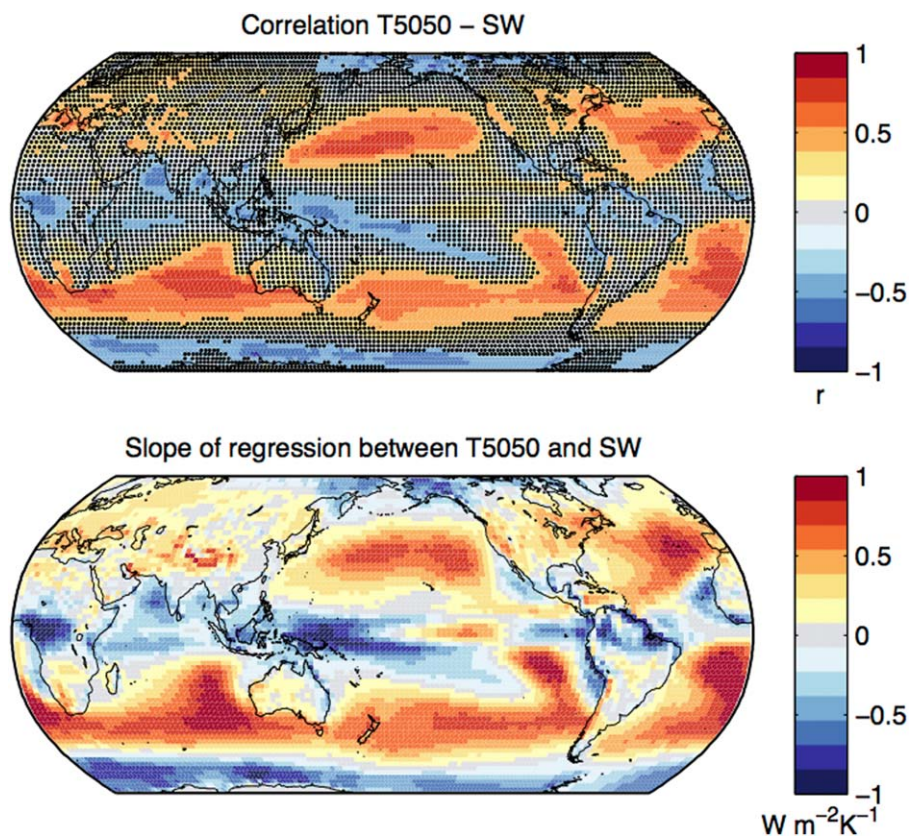
Figure 3. (top) The correlation coefficient (r) between the annual mean upwelling SW and the T5050 for each of the 26 models. Correlations that are not significant at 95% confidence are shown with black dots. (bottom) the slope of the across-model regression of T5050 and the annual-mean upwelling SW at each latitude and longitude. The units of the slope are W/m^2 of upwelling SW per degree K change in T5050.

[*Heymsfield et al.*, 2009; *Morrison et al.*, 2011]. Additionally, variations in GCM subtropical cloud cover are explained by processes that are not related to the mixed-phase parameterization [*Qu et al.*, 2014, 2015], which makes it hard to provide a convincing physical explanation for why such a persistent correlation between CF and T5050 exists across the CMIP5 model suite.

It seems plausible that the adjustment of either the cloud fraction or mixed-phase parameterizations to make the modeled SW reflection reasonably close to observations can lead to the correlation between T5050 and cloud fraction across the model ensemble. Because liquid generally has a smaller particle size and is more reflective than ice [*Heymsfield et al.*, 2003; *McCoy et al.*, 2014a], models that maintain a large amount of supercooled liquid must have a smaller mean-state low cloud cover in order that the SW cloud radiative effect is in reasonable agreement with observations. This is consistent with previous studies that have noted that GCMs tend to create clouds that are too few and too bright compared to observations over the stratocumulus regimes [*Bender et al.*, 2011; *Engstrom et al.*, 2014; *Nam et al.*, 2012].

3.2. Comparison to Observations

To examine the dependence of low cloud properties on mixed-phase parameterizations we consider the Southern Ocean. The Southern Ocean cloud cover in the control climate strongly affects the atmospheric general circulation in GCMs [*Frierson and Hwang*, 2012; *Hwang and Frierson*, 2013]. In addition, this region has extensive cloud cover [*Haynes et al.*, 2011; *McCoy et al.*, 2014a] and mixed-phase boundary layer cloud are prevalent [*Huang et al.*, 2012], making it ideal for examining the interactions of in-cloud LWP, cloud cover, and phase parameterizations between models.

The annual mean cloud-fraction-normalized LWP in the Southern Ocean (40°S–70°S) is negatively correlated with T5050 across the GCMs (Figure 6a). Models with a relatively low T5050 have clouds with a cloud-fraction-normalized LWP that is much higher than the observationally estimated range (Figure 6a). A
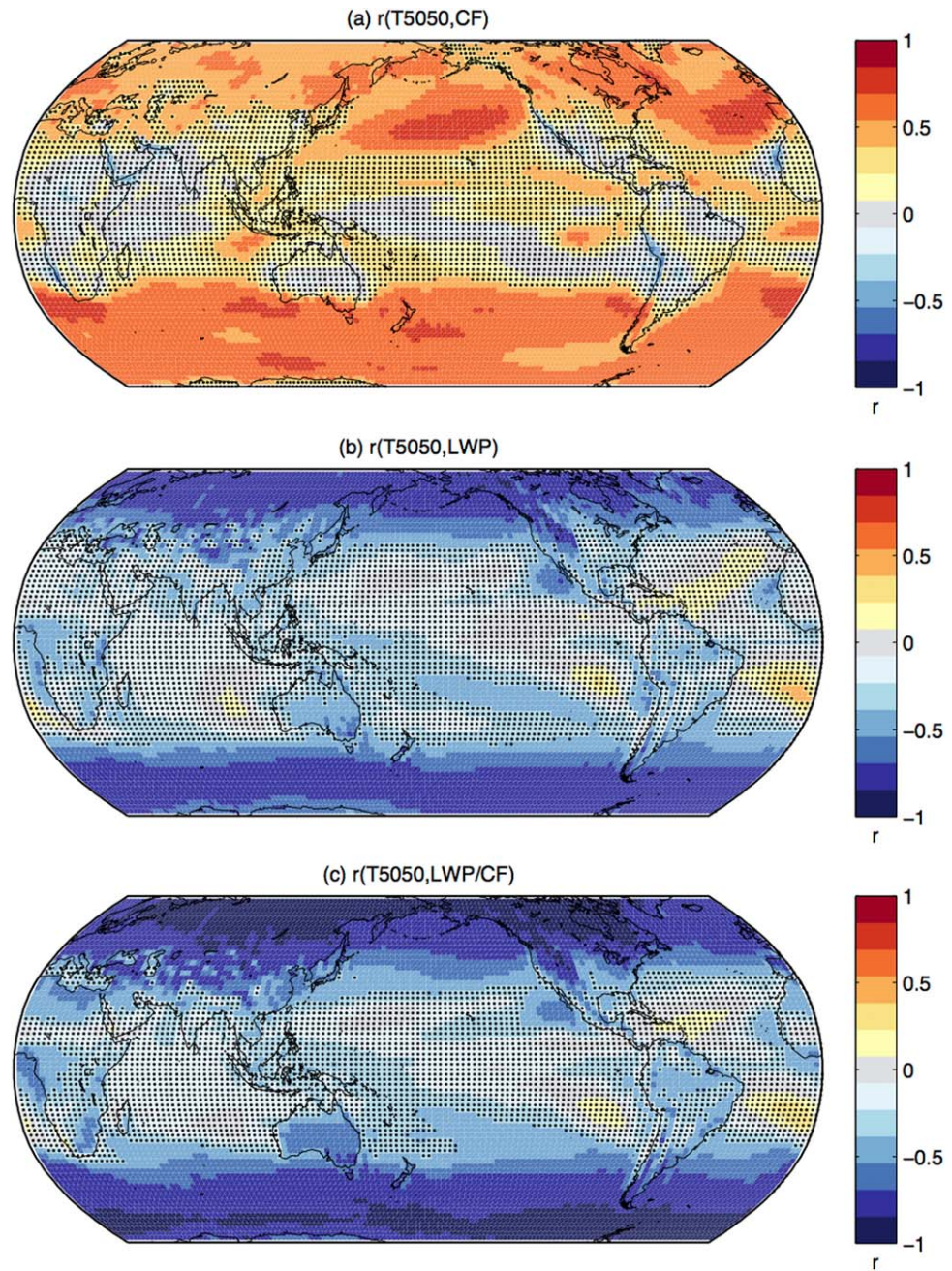
Figure 4. As in Figure 3, but showing the correlation between T5050 and cloud properties across models. The correlation coefficient is shown relating T5050 to (a) CF, (b) LWP, and (c) LWP normalized by CF.

positive correlation with CF (Figure 6c) and a negative correlation with LWP across models appear in the Southern Ocean (Figure 6b). The upwelling SW switches from being correlated with to anti-correlated with T5050 moving from the subtropics to the midlatitudes. Because of this switch the upwelling SW averaged over the 40°S–70°S region is not correlated with T5050 ($R^2=0.06$). Finally, over 60% of the intermodel variance in cloud-fraction-normalized LWP (Figure 6a) is explained by the variance in T5050 between models. This is a particularly surprising result given the diversity in the model representation of cloud cover [*Qu et al.*, 2014] and the relatively crude nature of the T5050 index used in this study.

Although the process level representation of mixed-phase cloud is complex [*Ceppi et al.*, 2015; *Klein et al.*, 2009; *Komurcu*, 2015; *Komurcu et al.*, 2014; *Morrison et al.*, 2011], we can utilize remote-sensing to offer a
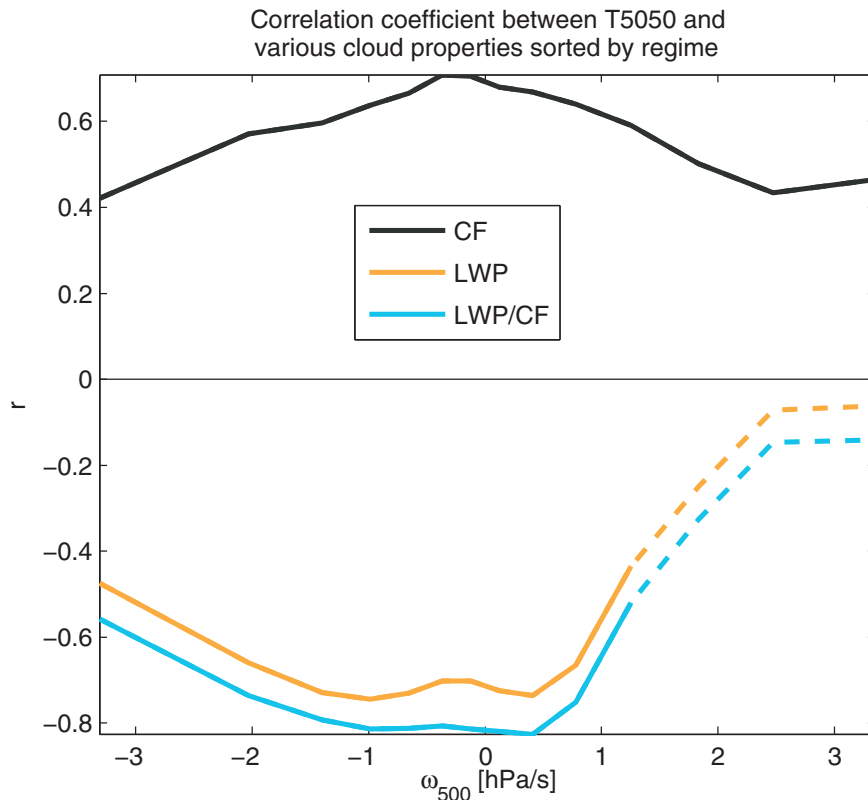
Figure 5. The correlation of T5050 with CF, LWP, and LWP/CF as a function of climatological, monthly pressure velocity at 500 hPa over the oceans. Correlations are taken using monthly climatologies from each model. Correlations that are significant at 95% confidence are shown using a solid line.

crude constraint on the in-cloud LWP and mixed-phase partitioning that is most in agreement with observations, indicating which models portray Southern Ocean low cloud less physically. The range of T5050 estimated from cloud lidar falls in the middle of the model diagnosed T5050s (Figures 1a and 6). Because the satellite lidar observations [*Hu et al.*, 2010] represent a global estimate of T5050 they are used to compare to model spread in Figure 6. As noted in the methods section, the CALIPSO-inferred T5050 does not represent a perfect comparison and the CALIPSO measurements of mixed-phase partitioning may have unknown systematic error, but it is consistent with the range of T5050s provided by surface-based lidar over a variety of aerosol regimes, and allows at least a loose constraint on GCM behavior. It is interesting to note that the historical range of mixed-phase partitioning inferred from regional aircraft observations of mixed-phase clouds roughly encompass the range of GCM behavior, while the surface-based lidar observations over a range of pristine and polluted regimes [*Kanitz et al.*, 2011] are more closely clustered around the CALIPSO data (Figure 1a), which is averaged over the globe as a whole.

We may also estimate the in-cloud LWP from observations. We provide two estimates of this quantity: the in-cloud LWP measured by MODIS, which excludes cloud edges, and the microwave LWP from UWISC divided by the cloud mask from MODIS. The range of LWP/CF given by these two different estimates is shown as a shaded bar in Figure 6a. Based on this estimate it appears that GCMs generally over-estimate the cloud-fraction-normalized LWP, despite generally not maintaining liquid to temperatures as low as those inferred from observations (Figure 1a). This overestimate of cloud-fraction-normalized LWP is consistent with previous investigations of cloud brightness and LWP [*Bender et al.*, 2011; *Engstrom et al.*, 2014; *Jiang et al.*, 2012; *Nam et al.*, 2012].

It is interesting that models do not appear to be able to represent the combination of cloud cover, LWP, and super-cooling that satellites observe in the current climate, even though their SW cloud radiative effect (CRE) is roughly consistent with CERES. Globally averaged SWCRE over oceans from the models surveyed in
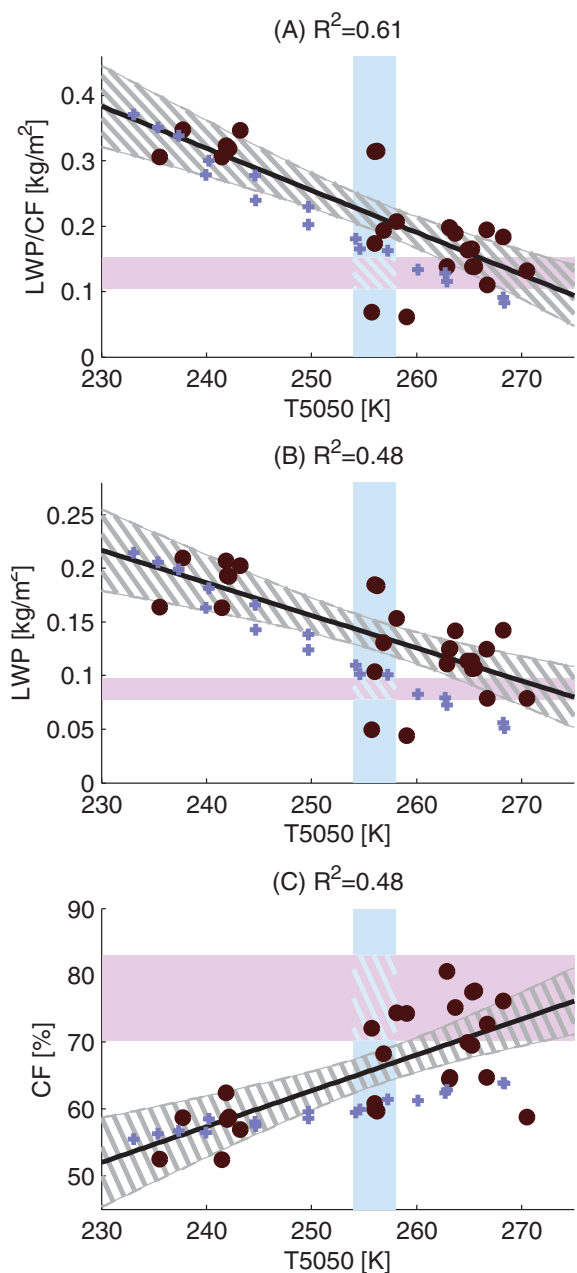
Figure 6. The correlation between annual mean values of LWP/CF, LWP, and CF averaged over the Southern Ocean between 40°S and 70°S. Each model is shown as a black dot. The fit of each variable to T5050 is shown as a black line with 95% confidence on the fit shown in the hatched area. The R^2 of the fit is noted in the title. Results from the perturbed physics experiments in CAM4 are shown using purple crosses. The range of different satellite-observed estimates of cloud properties and the estimate of T5050 are shown as blue and purple shading.

this study was between -54.7 Wm^{-2} and -40.5 Wm^{-2} with a median value of -49.8 Wm^{-2} and a standard deviation of 3 Wm-2. CERES EBAF TOA 2.8r estimates SWCRE over oceans as -47.15 Wm^{-2}. While the maximum difference between models is nearly 15 Wm^{-2}, the majority of the models are relatively close together.

It is unclear why the best-fit line of the models does not pass through the observationally estimated range of T5050 and LWP normalized by CF (Figure 6a). This may reflect an imperfect representation of the lidar analog of T5050, or it may indicate a systematic inability within GCMs to replicate the cloud microphysics that determine cloud albedo [*Ekman*, 2014; *Nam et al.*, 2012]. If an imperfect representation of cloud microphysics is to blame, it is consistent with the rapidly evolving observational understanding of both cloud microphysics and aerosol sources. Passive remote sensing of cloud droplet number concentration is still highly uncertain [*Cho et al.*, 2015; *Grosvenor and Wood*, 2014], and the sources of cloud condensation nuclei and ice nuclei in the pristine midlatitudes are still being determined [*Burrows et al.*, 2013; *McCoy et al.*, 2015b; *Quinn and Bates*, 2011; *Wilson et al.*, 2015].

Compensation between LWP and CF across models is not exclusive to the Southern Ocean. The across-model correlations relating SW to CF and in-cloud LWP have opposite signs at almost all latitudes (Figure 7). Models with larger CF tend to have greater reflected SW radiation at the TOA. This is sensible because, all else being equal, over a dark ocean more clouds will yield a larger reflected SW. However, models with larger in-cloud LWP and LWP tend to have less outgoing SW across the subtropics and midlatitudes, indicating that lower CF in these models over-compensates for higher in-cloud LWP. The upwelling SW and LWP/CF are positively correlated in the tropics. This is consistent with the melting level in convective clouds being affected by the mixed-phase parameterization.
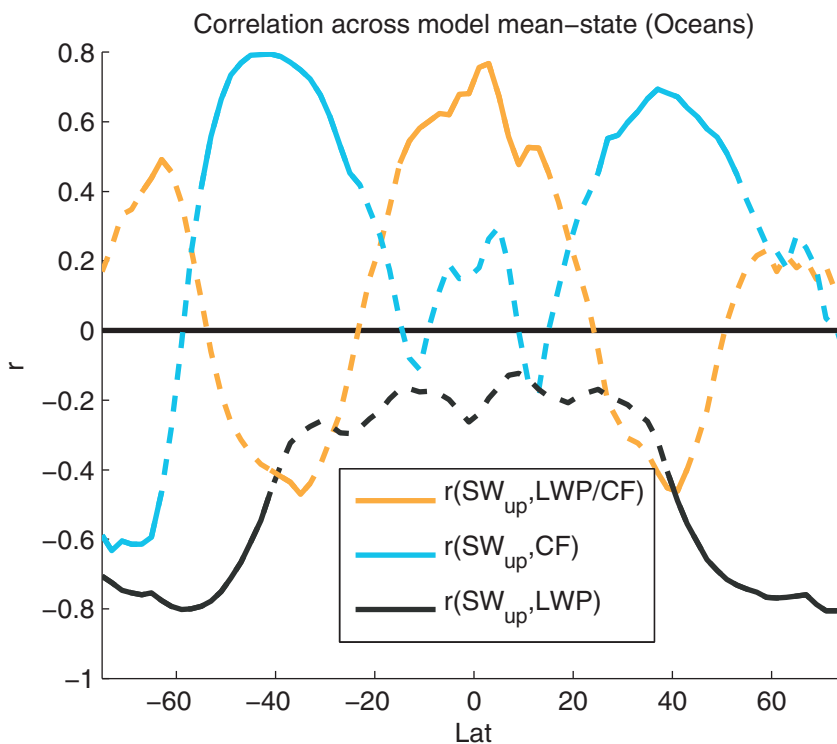
3.3. CAM4 Experiments

Based on the correlation between T5050 and cloud fraction described above (Figures 5 and 6c), it seems reasonable that critical relative humidity [*Quaas*, 2012], or other elements of the boundary layer cloud scheme in models that use more complex parameterizations [*Bender*, 2008; *Mauritsen et al.*, 2012; *Qu et al.*, 2014], are tuned so that global-mean SWCRE is within a few Wm^{-2} of the observed value (see above). Cloud

Figure 7. The across-model correlation relating zonal-mean upwelling SW to LWP and CF. Correlations that are significant at 95% confidence are shown using a solid line.

cover parameterizations are complex and it is difficult to compare diagnostically between models. To support the notion that the CMIP5 model behavior is originating from offsetting differences between the mixed-phase and cloud cover parameterizations we create a set of perturbed physics simulations in the Community Atmospheric Model Version 4 (CAM4).

We run CAM4 at $4° \times 5°$ horizontal resolution with fixed SST and a set of perturbed microphysics. CAM4 parameterizes mixed-phase physics and cloud cover in a highly idealized manner [*Gent et al.*, 2011; *Rasch and Kristjánsson*, 1998]. Ice and liquid condensate are partitioned linearly as a function of temperature, and the cloud fraction is evaluated based on a critical relative humidity threshold. We alter the phase partitioning function and critical relative humidity for low cloud formation to create an ensemble of CAM4 simulations where the T5050 spans the range of T5050 in the CMIP5 models. The mixed-phase partitioning in this ensemble has been adjusted so that the T5050s of the different realizations of CAM4 span 230 K–265 K. In each case, lower T5050 results in a higher SWCRE as in-cloud LWP increases. The critical relative humidity for low cloud formation is then altered in each simulation so that the global SWCRE stays approximately constant. Each perturbed physics simulation in CAM4 is run for two years with the finite volume dynamical core. In CAM4 cloud microphysics are prescribed so that the cloud droplet number concentration has fixed values over land, ocean, and ice. In our perturbed physics runs CAM4 is run with both the default marine cloud droplet number concentration (N_d) of 150 cm^{-3} and with a marine N_d of 50 cm^{-3}. The N_d over land and ice were kept at their default values. Details of the CAM4 runs are given in Table 2.

The across-ensemble member correlation between T5050 and upwelling SW is negative across the midlatitudes and convective tropics and positive across the subtropics (Figure 8). This pattern is qualitatively similar to the pattern of correlation between SW and T5050 seen across members in the CMIP5 ensemble (Figure 3). The correlation across the CAM4 ensemble members is stronger than across the CMIP5 models, but this is quite reasonable. All the CAM4 ensemble members have the same cloud parameterization with the exception of the critical RH, the marine N_d, and the mixed-phase partitioning. They also have approximately the same circulation because their SST is fixed. The CAM4 model is more idealized than many of the

Table 2. Details of the CAM4 Perturbed Physics Runs[a]

T5050 (K)	T_{max} (°C)	T_{min} (°C)	Critical RH	SWCRE (Wm^{-2})
Marine N_d = 150 cm^{-3}				
233.3	−20	−35	0.94	−55.2
235.5	−20	−30	0.95	−51.5
237.6	−15	−35	0.92	−54.5
240.4	−15	−30	0.91	−51.7
244.5	−10	−30	0.90	−55.6
249.5	−5	−30	0.89	−55.0
254.1	0	−30	0.88	−54.3
257.2	0	−20	0.86	−54.5
262.7	0	−15	0.85	−54.9
268.3	0	−5	0.83	−54.0
Marine N_d = 50 cm^{-3}				
240.1	−15	−30	0.93	−51.6
244.6	−10	−30	0.92	−51.3
249.5	−5	−30	0.89	−54.2
254.5	0	−30	0.88	−53.4
260.1	0	−20	0.86	−53.7
262.9	0	−15	0.85	−54.3
268.4	0	−5	0.83	−53.3

[a]The T5050, values that set the temperature ramp, critical RH, and SWCRE are listed for each run. The total condensate is decomposed into liquid and ice following a temperature ramp. The fraction of ice, f_i, is parameterized as $f_i = \frac{T - T_{max}}{T_{min} - T_{max}}$. The table is seperated into runs that used the default value of marine Nd of 150 cm^{-3} or the perturbed value of 50 cm^{-3}.

newer CMIP5 models, but the similarity in the pattern is striking and supports the notion that mixed-phase cloud parameterizations are leading to strong local biases in mean SW flux.

The in-cloud LWP generated by the CAM4 simulations exhibits the same behavior as the 26 GCMs from CMIP5 in the 40°S–70°S latitude band (purple crosses in Figure 6a). The CAM4 LWP is negatively correlated with T5050 and the CAM4 CF is positively correlated with T5050. This is consistent with the behavior of the CMIP5 model ensemble. It is interesting to note that the CAM4 ensemble members' CF appear to be less dependent on T5050 than the CMIP5 models, and the LWP is more strongly dependent on T5050. The sign of the trends is reproduced and the positive correlation between T5050 and SW in the subtropics is quite strong. This demonstrates that the covariances across the CMIP5 model ensemble can be replicated in a single model by compensating enhancements in supercooled liquid and decreases in global cloud fraction if the upwelling SW is held fixed.

3.4. Cloud Feedbacks

It is unclear how artificially compensating mixed-phase cloud and cloud fraction parameterizations would affect the climate system as a whole. This behavior is worrisome from the perspective of constraining the model representation of climate and climate change. The control climate TOA albedo over the Southern Ocean and in the subtropical stratocumulus-to-cumulus transition region have been shown to correlate with climate sensitivity and changes in atmospheric circulation in GCMs [*Frierson and Hwang*, 2012; *Grise et al.*, 2015; *Hwang and Frierson*, 2013; *Trenberth and Fasullo*, 2010]. However, in the Southern Ocean (40°S–70°S) the cloud cover transitions from warm to mixed-phase clouds with increasing latitude. In the warm clouds, reflected SW is correlated with T5050 through increasing CF and in the mixed-phase clouds, reflected SW is anti-correlated with T5050 through decreasing in-cloud LWP (Figures 3 and 4). This makes the Southern Ocean upwelling SW averaged over the 40°S–70°S region uncorrelated with T5050.

Correlation T5050–SW CAM4 perturbed physics
n= 17
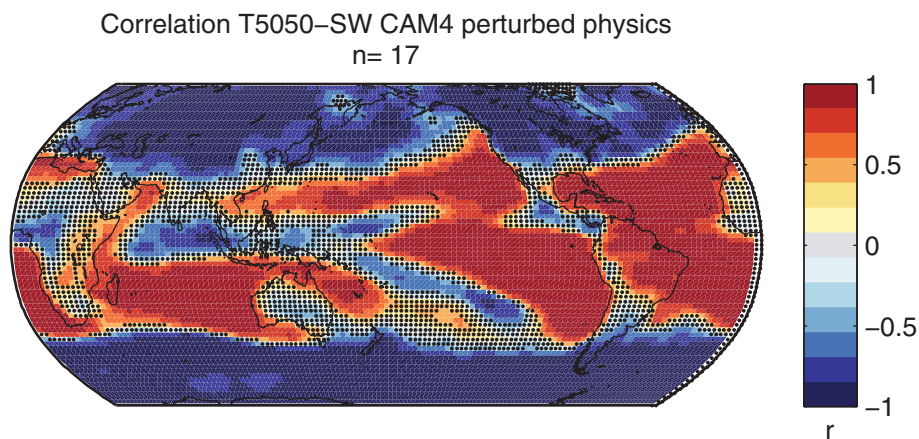
Figure 8. As in Figure 3, but for the 17 ensemble members of CAM4 run with perturbed liquid and ice partitioning and fixed SST (see Table 2).
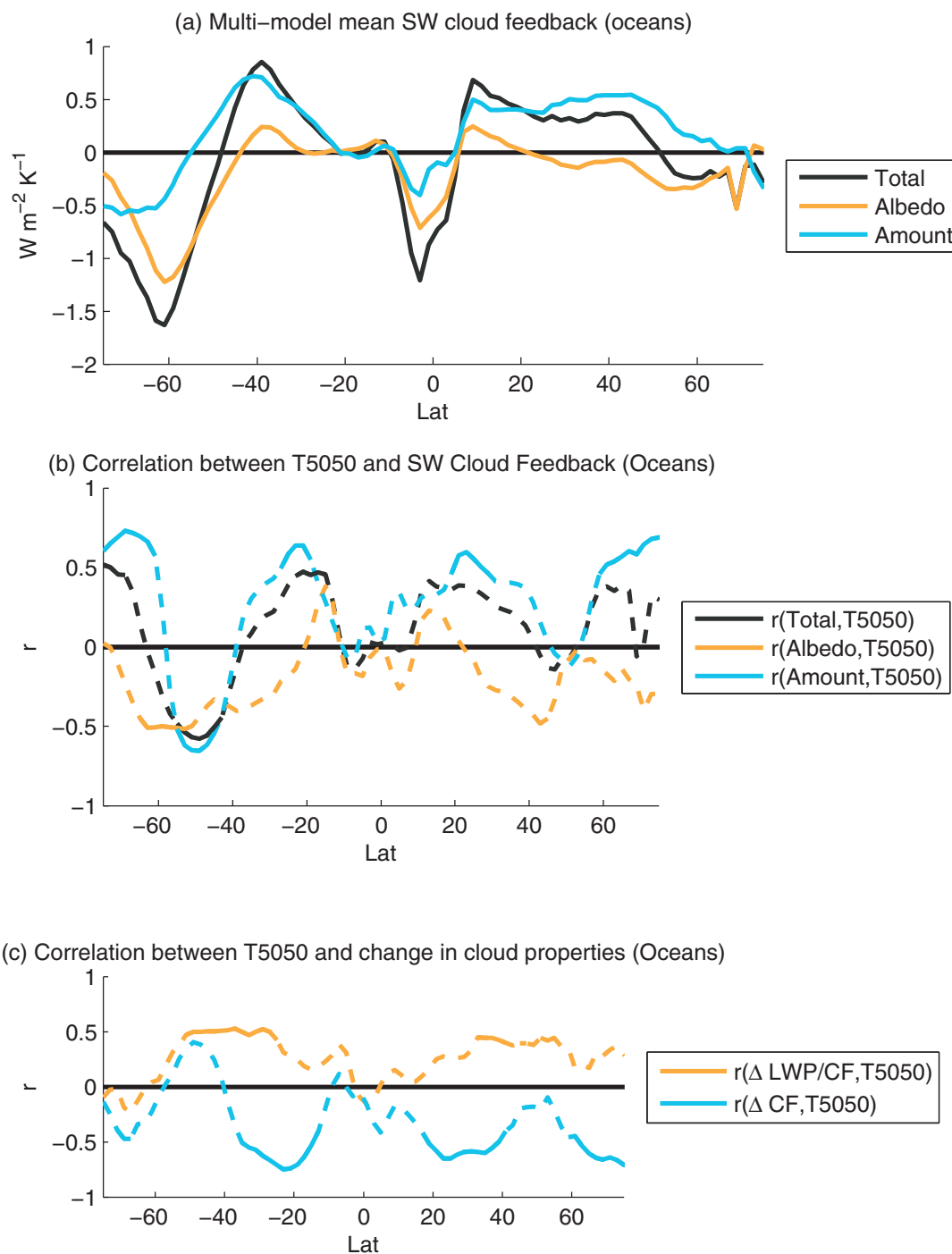
Figure 9. (a) The zonal, multimodel mean APRP SW cloud feedback and the contributions to the SW cloud feedback from changes in amount and albedo, which is analogous to optical depth. The zonal mean is only taken over oceans. (b) The correlation coefficient between each GCM's T5050 and zonal-mean APRP SW cloud feedback. The correlation coefficients between T5050 and the amount and albedo contributions to the cloud feedback are also shown. (c) The correlation between T5050 and changes in cloud-fraction-normalized LWP and CF between the historical and RCP8.5 simulations normalized by changes in local surface temperature. If the correlation coefficient is significant at 95% confidence a solid line is used.

We will now discuss how model mixed-phase behavior appears to influence the cloud feedback. The GCM-predicted LWP increase with warming that drives the robust negative optical depth cloud feedback at high latitudes (Figure 9a) [*Gordon and Klein*, 2014; *Kay et al.*, 2014; *Zelinka et al.*, 2012, 2013] has been shown to
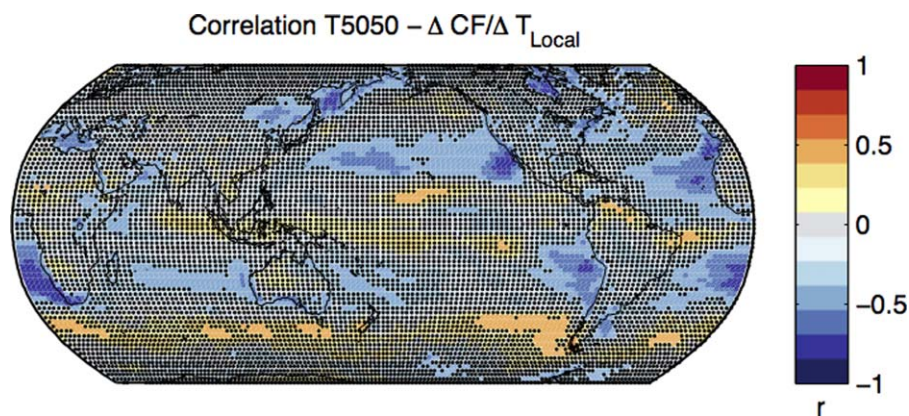
Figure 10. As in Figure 3, but showing the across-model correlation between T5050 and changes in CF. Changes in CF are normalized by the change in local surface temperature.

exhibit a strong dependence on model T5050 [*McCoy et al.*, 2015a]. Based on this mechanism we evaluate the dependence of SW cloud feedback on T5050. Models with higher T5050 tend to have more negative SW cloud feedback at higher latitudes and a more positive feedback across the subtropics (Figure 9b). Using CMIP5 abrupt4xCO2 simulations and the APRP technique of *Taylor et al.* [2007], we compute the SW cloud feedback and its contributions from changes in cloud albedo and from changes in cloud amount.

The SW cloud albedo feedback, which is roughly equivalent to the SW cloud optical depth feedback [see *Zelinka et al.*, 2012], is negatively correlated with T5050 at all latitudes. The negative correlation between cloud albedo feedback and T5050 is consistent with the idea that models that have more ice in their mean state will brighten more in a warming climate as their ice transitions to liquid [*McCoy et al.*, 2014b, 2015a; *Zelinka et al.*, 2012]. To support this analysis we compare the cloud feedback to the change in cloud properties between the historical and RCP8.5 simulations. The change in estimated in-cloud LWP, normalized by local change in surface temperature, is positively correlated with T5050 at virtually all latitudes (Figure 9c). This is consistent with changes in cloud LWP driving the increase in cloud albedo. For higher T5050s the latitude where ice transitions to liquid is more equatorward. Since the insolation is stronger in these regions, the increase in reflected SW from a given albedo increase is greater. That is to say, higher T5050 gives you more ice to transition as the climate warms everywhere, and also causes the ice-to-liquid transition to occur further equatorward where there is more sunlight to reflect.

The amount component of the SW cloud feedback is correlated both positively and negatively with T5050, depending on latitude (Figure 9b). A negative correlation between the SW cloud amount feedback and T5050 is somewhat reasonable in regions of persistent mixed-phase clouds such as the Southern Ocean. As GCMs transition to being more liquid dominated the cloud fraction should increase due a decrease in efficient ice precipitation [*Morrison et al.*, 2011]. GCMs with a higher T5050 will have more ice to transition to liquid as the climate warms. The sign of the correlation in the Southern Hemisphere shifts from negative in the midlatitudes to positive in the subtropics. As the climate warms, models with a high T5050 tend to both decrease their subtropical cloud cover more strongly and enhance their Southern Ocean cloud cover more strongly (Figure 9c). Changes in cloud cover appear to be most strongly negatively correlated with T5050 in the stratocumulus regions [see *Klein and Hartmann*, 1993] (Figure 10). Because there is no clear physical mechanism to explain the linkage between subtropical liquid cloud and the mixed-phase parameterization, it seems likely that this behavior is a byproduct of tuning of some global cloud-cover-controlling parameter to compensate for albedo variations engendered by model mixed-phase parameterization.

Many parameters may be tuned to bring a GCM into top of atmosphere energy balance [*Bender*, 2008; *Mauritsen et al.*, 2012] and singling out a parameter that has been tuned is difficult. It is interesting to note that RH tends to decrease over subsidence regions and increase over ascent regions in global warming simulations (Figure 11). This behavior is similar across GCMs [*Wright et al.*, 2010]. The pattern of drying and moistening is qualitatively consistent with the pattern of correlation between T5050 and changes in cloud fraction in GCMs (Figure 10). It is possible that this correlation may be explained by positive feedbacks between boundary-layer cloud radiative cooling, relative humidity, and cloud cover as described by *Brient*
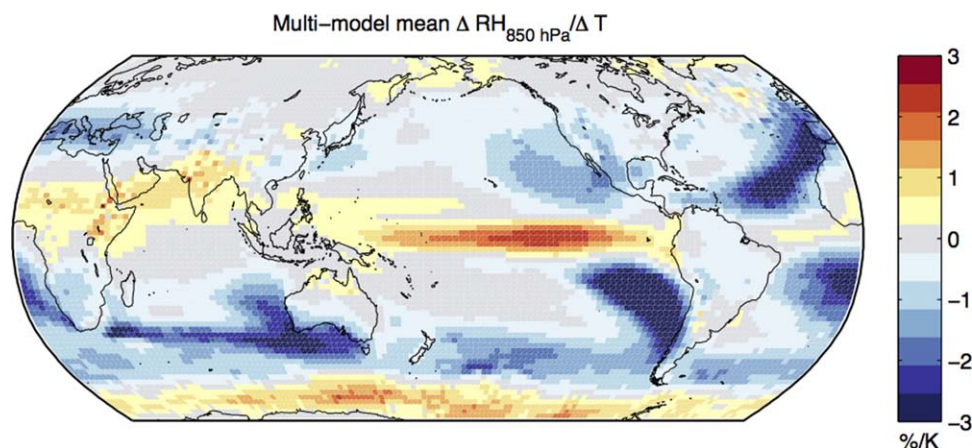
Figure 11. The multimodel mean change in RH at 850 hPa between the historical and RCP8.5 simulations. Changes in RH are normalized by the local change in surface temperature.

and Bony [2012]. This set of feedbacks resulted in a stronger reduction in low cloud cover in models where the climate mean-state cloud cover was higher. However, there is unlikely to be a single unifying mechanism linking T5050 to changes in cloud cover across all the CMIP5 models. Low cloud cover in GCMs and observations is sensitive to several environmental factors with widely varying strengths across models [*Myers and Norris*, 2014, 2016; *Qu et al.*, 2015], making it difficult to isolate the role of any given parameterization [*Bender*, 2008; *Mauritsen et al.*, 2012].

Regardless of the parameterization process, in high T5050 GCMs for which ice exists at warmer temperatures; climate mean state cloud fraction is uniformly higher; subtropical cloud cover decreases more; and Southern Ocean cloud cover increases more. It appears that this behavior is linked to tuning of some global cloud cover-controlling parameter to compensate for the choice of mixed-phase parameterization in a given GCM.

It is interesting to note that the remote sensing-inferred range of T5050 [*Cesana et al.*, 2015; *Hu et al.*, 2010] shows that a substantial fraction of the CMIP5 models do not maintain liquid to sufficiently low temperatures (Figure 1a), indicating that the SW cloud optical depth feedback is likely to be less negative than implied by the CMIP5 ensemble. This is consistent with the conclusions of *Gordon and Klein* [2014]. Similarly, GCMs with a higher T5050 have a more positive subtropical cloud amount feedback, however the linkage between these model features appears to be artificial, in contrast to the linkage between the optical depth feedback and T5050. That is, if the linkage between cloud cover and T5050 was based on some sort of physical process we could hypothesize that excluding models with T5050s outside of the observational range would yield a reasonable range for the cloud amount feedback [*Klein and Hall*, 2015]. However, the linkage between T5050 and cloud amount feedback appears to be through the tuning of the climate mean-state cloud fraction to compensate for variations in midlatitude cloud albedo engendered by mixed-phase parameterizations. Thus, the most reasonable range of T5050 does not give us any insight into the most reasonable cloud amount feedback. In summary, our conclusion that the midlatitude mixed-phase negative feedback is too strong in models, coupled with the growing body of observational evidence supporting a robustly positive cloud amount feedback in the subtropics [*Bretherton and Blossey*, 2014; *Clement et al.*, 2009; *Eastman et al.*, 2011; *Myers and Norris*, 2014, 2016; *Qu et al.*, 2014, 2015], suggests that total SW cloud feedback is positive globally.

4. Conclusions

We examine a wide selection of the GCMs from CMIP5 in relation to their cloud properties and mixed-phase behavior. GCMs effectively partition ice and liquid cloud condensate as a monotonic function of atmospheric temperature. This partitioning is highly variable between models (Figure 1a). The temperature where cloud ice and liquid are equally abundant (T5050) was used to typify the mixed-phase behavior in each model. The inter-model spread in T5050 was found to explain a large amount of the variance
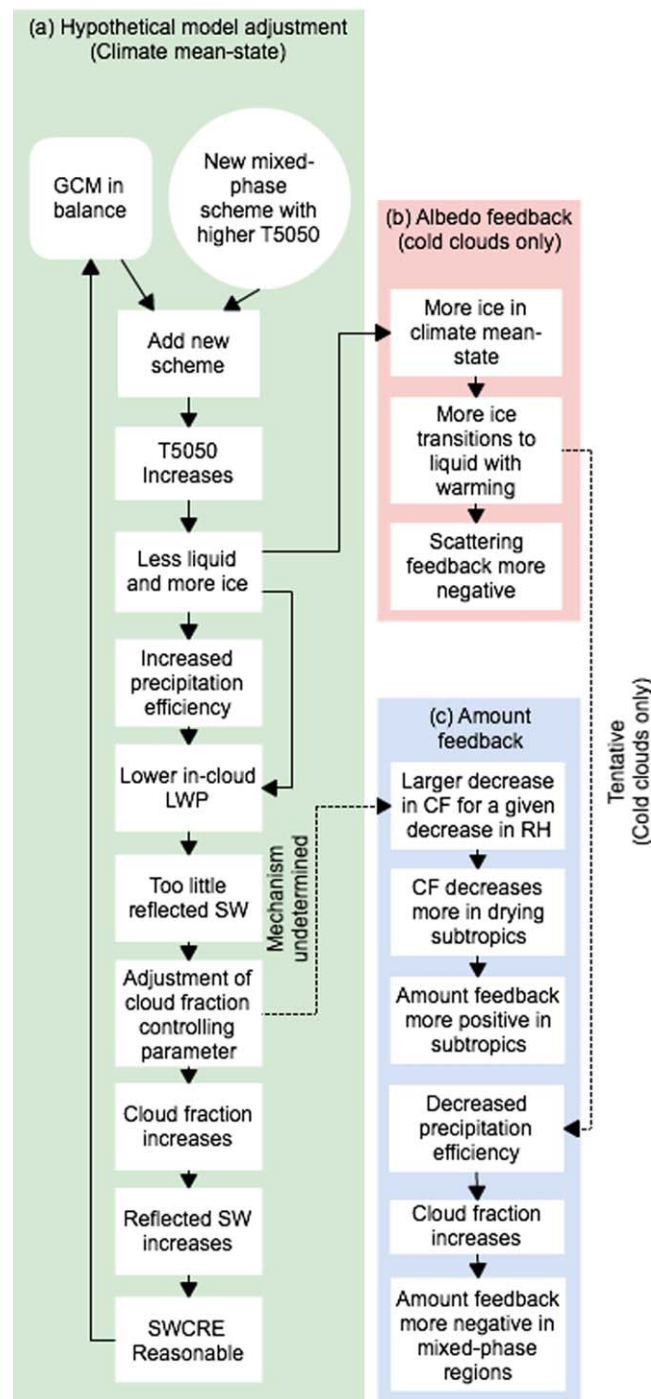
Figure 12. A flow chart describing the mechanisms discussed in this study that are hypothesized to link GCM mixed-phase parameterization (characterized as T5050) to the representation of (a) mean-state cloud properties, (b) the albedo feedback, and (c) the cloud amount feedback. The explanation is given in the context of an increase in T5050 in a hypothetical GCM. The effects on climate mean-state cloud properties and cloud feedbacks due to this perturbation in T5050 are described by the flow chart.

in cloud fraction and LWP across models (Figure 5). While the robust negative correlation between T5050 and LWP is very sensible (if T5050 is high then liquid is not maintained at low temperatures), the strong positive correlation between CF and T5050 appears to be a product of model tuning, rather than physical processes that might occur in nature. If cloud fraction and mixed-phase properties are coupled, observations indicate that the correlation between glaciation and cloud fraction should be negative [*Heymsfield et al.*, 2009; *Morrison et al.*, 2011]. The correlation between CF and T5050 is robustly positive across subsidence regimes and geographic regions, including the subtropics (Figures 4a and 5). This behavior results in the T5050 correlating positively with upwelling SW across the subtropics and negatively across the midlatitudes (Figure 3).

The Southern Ocean (40°S–70°S) is analyzed in the context of model mixed-phase behavior and it is shown that models that do not maintain liquid at lower temperatures tend to have more cloud cover, but less in-cloud liquid. It seems likely that the cloud cover parameterization is being tuned in such a way as to compensate for the mixed-phase parameterization of each model, creating fewer clouds that contain too much liquid water. That is to say, "too few, too bright" [*Nam et al.*, 2012] can plausibly be explained as a byproduct of tuning cloud fraction to compensate for unrealistic mixed-phase clouds.

A set of perturbed physics CAM4 simulations are performed in which T5050 is set to values across a range like that shown by the CMIP5 model ensemble, and the critical relative humidity for low cloud formation is tuned so that the SWCRE is consistent with observations from CERES. This suite of CAM4 experiments replicates the dependence of cloud fraction and liquid content on T5050 (Figure 6), suggesting that the critical relative humidity may be artificially high to compensate for clouds that are too bright in models with low T5050s (Figure 4). However, it should be noted that many other parameters could be tuned to alter CF [*Bender*, 2008;

Mauritsen et al., 2012]. A diagram summarizing the hypothesized mechanisms linking T5050 and climate mean-state cloud properties is shown in Figure 12a.

In addition to affecting the climate mean-state, mixed-phase parameterizations appear to affect SW cloud feedbacks. A diagram summarizing the mechanisms hypothesized to link T5050 to cloud feedbacks is provided in Figures 12b and 12c. The cloud amount component of the SW cloud feedback correlates both positively and negatively with T5050, depending on region. One might reasonably expect that, holding all other predictors of cloud cover constant, cloud amount in the persistently mixed-phase regions would increase as the climate warms due to mixed-phase clouds becoming liquid dominated (a negative feedback) [*Heymsfield et al.*, 2009; *Morrison et al.*, 2011]. This implies that models that glaciate more readily will have a larger increase in cloud fraction as readily precipitable ice is replaced with liquid in a warming climate. This is consistent with the Southern Ocean cloud amount feedback where mixed-phase clouds are prevalent (Figure 9). A stronger decrease in cloud fraction across the subtropics in models that glaciate more readily does not have a robust physical explanation, much less one that would be implemented across the CMIP5 models. However, it does appear that models with higher climate mean-state cloud cover tend to decrease their cloud cover more strongly as the climate warms [*Brient and Bony*, 2012]. It seems likely that across-model covariances between T5050 and cloud-coverage-controlling parameters among GCMs lead to a stronger decrease in subtropical cloud cover as the climate warms in high T5050 models.

The SW cloud albedo feedback correlates negatively with T5050 through the mid and high latitudes (Figure 9). This is sensible because GCMs with more ice in their control climates will be able to transition more ice to liquid. Because liquid is more reflective than ice this results in a negative SW cloud albedo feedback. While it is important to keep in mind that the observational mixed-phase partitionings shown in Figure 1a are not directly analogous to the GCM T5050, a large number of GCMs (12/26) considered in this study have a higher T5050 than inferred from either satellite observations or the most polluted continental ground-based lidar observations. This indicates that the cloud albedo feedback in the mid and high latitudes may be unrealistically negative in GCMs. This is consistent with the conclusions presented by *Gordon and Klein* [2014].

Overall, it is likely that the broad range in mixed-phase parameterizations and compensating changes in cloud fraction strongly affect the cloud properties in both the control and perturbed climates simulated by GCMs. To the extent that the compensation between positive subtropical cloud amount feedback and negative midlatitude optical depth feedback is spurious, the SW cloud feedback may be constrained to an artificially small range in CMIP5. It is evident that mixed-phase parameterizations must be more carefully vetted in the next generation of GCMs to reduce regional albedo biases and narrow the uncertainty in cloud feedback and climate sensitivity.

References

Atkinson, J. D., B. J. Murray, M. T. Woodhouse, T. F. Whale, K. J. Baustian, K. S. Carslaw, S. Dobbie, D. O'Sullivan, and T. L. Malkin (2013), The importance of feldspar for ice nucleation by mineral dust in mixed-phase clouds, *Nature*, *498*(7454), 355–358.

Bender, F. A. M. (2008), A note on the effect of GCM tuning on climate sensitivity, *Environ. Res. Lett.*, *3*(1), 014001.

Bender, F. A. M., R. J. Charlson, A. M. L. Ekman, and L. V. Leahy (2011), Quantification of monthly mean regional-scale albedo of marine stratiform clouds in satellite observations and GCMs, *J. Appl. Meteorol. Climatol.*, *50*(10), 2139–2148.

Blossey, P. N., C. S. Bretherton, M. H. Zhang, A. N. Cheng, S. Endo, T. Heus, Y. G. Liu, A. P. Lock, S. R. de Roode, and K. M. Xu (2013), Marine low cloud sensitivity to an idealized climate change: The CGILS LES intercomparison, *J. Adv. Model. Earth Syst.*, *5*, 234–258. doi:10.1002/jame.20025.

Bony, S., J. L. Dufresne, H. Le Treut, J. J. Morcrette, and C. Senior (2004), On dynamic and thermodynamic components of cloud changes, *Clim. Dyn.*, *22*(2-3), 71–86.

Bony, S., et al. (2006), How well do we understand and evaluate climate change feedback processes?, *J. Clim.*, *19*(15), 3445–3482.

Bower, K. N., S. J. Moss, D. W. Johnson, T. W. Choularton, J. Latham, P. R. A. Brown, A. M. Blyth, and J. Cardwell (1996), A parametrization of the ice water content observed in frontal and convective clouds, *Q. J. R. Meteorol. Soc.*, *122*(536), 1815–1844.

Bretherton, C. S., and P. N. Blossey (2014), Low cloud reduction in a greenhouse-warmed climate: Results from Lagrangian LES of a subtropical marine cloudiness transition, *J. Adv. Model. Earth Syst.*, *6*, 91–114, doi:10.1002/2013MS000250.

Bretherton, C. S., P. N. Blossey, and C. R. Jones (2013), Mechanisms of marine low cloud sensitivity to idealized climate perturbations: A single-LES exploration extending the CGILS cases, *J. Adv. Model. Earth Syst.*, *5*, 316–337, doi:10.1002/jame.20019.

Brient, F., and S. Bony (2012), How may low-cloud radiative properties simulated in the current climate influence low-cloud feedbacks under global warming?, *Geophys. Res. Lett.*, *39*, L20807, doi:10.1029/2012GL053265.

Brient, F., and S. Bony (2013), Interpretation of the positive low-cloud feedback predicted by a climate model under global warming, *Clim. Dyn.*, *40*(9-10), 2415–2431.

Brient, F., T. Schneider, Z. Tan, S. Bony, X. Qu, and A. Hall (2015), Shallowness of tropical low clouds as a predictor of climate models' response to warming, *Clim. Dyn.*, 1–17.

Burrows, S. M., C. Hoose, U. Poschl, and M. G. Lawrence (2013), Ice nuclei in marine air: Biogenic particles or dust?, *Atmos. Chem. Phys.*, *13*(1), 245–267.

Ceppi, P., D. L. Hartmann, and M. J. Webb (2015), Mechanisms of the negative shortwave cloud feedback in mid to high latitudes, *J. Clim.*, *29*(1), 139–157, doi:10.1175/JCLI-D-15-0327.1.

Cesana, G., D. E. Waliser, X. Jiang, and J. L. F. Li (2015), Multi-model evaluation of cloud phase transition using satellite and reanalysis data, *J. Geophys. Res. Atmos.*, *120*, 7871–7892, doi:10.1002/2014JD022932.

Cho, H.-M., et al. (2015), Frequency and causes of failed MODIS cloud property retrievals for liquid phase clouds over global oceans, *J. Geophys. Res. Atmos.*, *120*, 4132–4154, doi:10.1002/2015JD023161.

Choi, Y. S., C. H. Ho, C. E. Park, T. Storelvmo, and I. Tan (2014), Influence of cloud phase composition on climate feedbacks, *J. Geophys. Res. Atmos.*, *119*, 3687–3700, doi:10.1002/2013JD020582.

Clement, A. C., R. Burgman, and J. R. Norris (2009), Observational and model evidence for positive low-level cloud feedback, *Science*, *325*(5939), 460–464.

Cober, S. G., G. A. Isaac, A. V. Korolev, and J. W. Strapp (2001), Assessing cloud-phase conditions, *J. Appl. Meteorol.*, *40*(11), 1967–1983.

Dufresne, J. L., and S. Bony (2008), An assessment of the primary sources of spread of global warming estimates from coupled atmosphere-ocean models, *J. Clim.*, *21*(19), 5135–5144.

Eastman, R., S. G. Warren, and C. J. Hahn (2011), Variations in cloud cover and cloud types over the ocean from surface observations, 1954–2008, *J. Clim.*, *24*(22), 5914–5934.

Ekman, A. M. L. (2014), Do sophisticated parameterizations of aerosol-cloud interactions in CMIP5 models improve the representation of recent observed temperature trends?, *J. Geophys. Res. Atmos.*, *119*, 817–832, doi:10.1002/2013JD020511.

Engstrom, A., F. A. M. Bender, and J. Karlsson (2014), Improved representation of marine stratocumulus cloud shortwave radiative proper-ties in the CMIP5 climate models, *J. Clim.*, *27*(16), 6175–6188.

Frierson, D. M. W., and Y. T. Hwang (2012), Extratropical influence on ITCZ shifts in slab ocean simulations of global warming, *J. Clim.*, *25*(2), 720–733.

Gent, P. R., et al. (2011), The community climate system model version 4, *J. Clim.*, *24*(19), 4973–4991.

Gordon, N. D., and S. A. Klein (2014), Low-cloud optical depth feedback in climate models, *J. Geophys. Res. Atmos.*, *119*, 6052–6065, doi:10.1002/2013JD021052.

Grise, K. M., L. M. Polvani, and J. T. Fasullo (2015), Re-examining the relationship between climate sensitivity and the Southern Hemisphere radiation budget in CMIP models, *J. Clim.*, *28*, 9298–9312.

Grosvenor, D. P., and R. Wood (2014), The effect of solar zenith angle on MODIS cloud optical and microphysical retrievals within marine liquid water clouds, *Atmos. Chem. Phys.*, *14*(14), 7291–7321.

Haynes, J. M., C. Jakob, W. B. Rossow, G. Tselioudis, and J. Brown (2011), Major characteristics of southern ocean cloud regimes and their effects on the energy budget, *J. Clim.*, *24*(19), 5061–5080.

Heymsfield, A. J., S. Matrosov, and B. Baum (2003), Ice water path-optical depth relationships for cirrus and deep stratiform ice cloud layers, *J. Appl. Meteorol.*, *42*(10), 1369–1390.

Heymsfield, A. J., P. C. Kennedy, S. Massie, C. Schmitt, Z. Wang, S. Haimov, and A. Rangno (2009), Aircraft-induced hole punch and canal clouds: Inadvertent cloud seeding, *Bull. Am. Meteorol. Soc.*, *91*(6), 753–766.

Hu, Y., S. Rodier, K. Xu, W. Sun, J. Huang, B. Lin, P. Zhai, and D. Josset (2010), Occurrence, liquid water content, and fraction of supercooled water clouds from combined CALIOP/IIR/MODIS measurements, *J. Geophys. Res.*, *115*, D00H34, doi:10.1029/2009JD012384.

Huang, Y., S. T. Siems, M. J. Manton, A. Protat, and J. Delanoe (2012), A study on the low-altitude clouds over the Southern Ocean using the DARDAR-MASK, *J. Geophys. Res.*, *117*, D18204, doi:10.1029/2012JD017800.

Hwang, Y. T., and D. M. W. Frierson (2013), Link between the double-Intertropical Convergence Zone problem and cloud biases over the Southern Ocean, *Proc. Natl. Acad. Sci. U. S. A.*, *110*(13), 4935–4940.

Isaac, G. A., and R. S. Schemenauer (1979), Large particles in supercooled regions of northern Canadian Cumulus Clouds, *J. Appl. Meteorol.*, *18*(8), 1056–1065.

Jiang, J. H., et al. (2012), Evaluation of cloud and water vapor simulations in CMIP5 climate models using NASA ''A-Train'' satellite observa-tions, *J. Geophys. Res.*, *117*, D14105, doi:10.1029/2011JD017237.

Kanitz, T., P. Seifert, A. Ansmann, R. Engelmann, D. Althausen, C. Casiccia, and E. G. Rohwer (2011), Contrasting the impact of aerosols at northern and southern midlatitudes on heterogeneous ice formation, *Geophys. Res. Lett.*, *38*, L17802, doi:10.1029/2011GL048532 .

Kay, J. E., B. Medeiros, Y. T. Hwang, A. Gettelman, J. Perket, and M. G. Flanner (2014), Processes controlling Southern Ocean shortwave cli-mate feedbacks in CESM, *Geophys. Res. Lett.*, *41*, 616–622, doi:10.1002/2013GL058315.

Klein, S. A., and A. Hall (2015), Emergent constraints for cloud feedbacks, *Curr. Clim. Change Rep.*, *1*, 1–12.

Klein, S. A., and D. L. Hartmann (1993), The seasonal cycle of low stratiform clouds, *J. Clim.*, *6*(8), 1587–1606.

Klein, S. A., D. L. Hartmann, and J. R. Norris (1995), On the relationships among low-cloud structure, sea surface temperature, and atmos-pheric circulation in the summertime Northeast Pacific, *J. Clim.*, *8*(5), 1140–1155.

Klein, S. A., et al. (2009), Intercomparison of model simulations of mixed-phase clouds observed during the ARM Mixed-Phase Arctic Cloud Experiment. I: Single-layer cloud, *Q. J. R. Meteorol. Soc.*, *135*(641), 979–1002.

Komurcu, M. (2015), Influences of ice crystal number concentrations and habits on arctic mixed-phase cloud dynamics, *Pure Appl. Geophys.*, 1–16.

Komurcu, M., T. Storelvmo, I. Tan, U. Lohmann, Y. X. Yun, J. E. Penner, Y. Wang, X. H. Liu, and T. Takemura (2014), Intercomparison of the cloud water phase among global climate models, *J. Geophys. Res. Atmos.*, *119*, 3372–3400, doi:10.1002/2013JD021119.

Korolev, A. V., G. A. Isaac, S. G. Cober, J. W. Strapp, and J. Hallett (2003), Microphysical characterization of mixed-phase clouds, *Q. J. R. Mete-orol. Soc.*, *129*(587), 39–65.

Marchand, R., T. Ackerman, M. Smyth, and W. B. Rossow (2010), A review of cloud top height and optical depth histograms from MISR, ISCCP, and MODIS, *J. Geophys. Res.*, *115*, D16206, doi:10.1029/2009JD013422.

Mauritsen, T., et al. (2012), Tuning the climate of a global model, *J. Adv. Model. Earth Syst.*, *4*, M00A01, doi:10.1029/2012MS000154.

McCoy, D. T., D. L. Hartmann, and D. P. Grosvenor (2014a), Observed southern ocean cloud properties and shortwave reflection. Part I: Cal-culation of SW Flux from observed cloud properties, *J. Clim.*, *27*(23), 8836–8857.

McCoy, D. T., D. L. Hartmann, and D. P. Grosvenor (2014b), Observed southern ocean cloud properties and shortwave reflection. Part II: Phase changes and low cloud feedback, *J. Clim.*, *27*(23), 8858–8868.

McCoy, D. T., D. L. Hartmann, M. D. Zelinka, P. Ceppi, and D. P. Grosvenor (2015a), Mixed-phase cloud physics and Southern Ocean cloud feedback in climate models, *J. Geophys. Res. Atmos.*, *120*, 9539–9554, doi:10.1002/2015JD023603.

McCoy, D. T., S. M. Burrows, R. Wood, D. P. Grosvenor, S. M. Elliott, P.-L. Ma, P. J. Rasch, and D. L. Hartmann (2015b), Natural aerosols explain seasonal and spatial patterns of Southern Ocean cloud albedo, *Sci. Adv.*, *1*(6).

Morrison, H., G. de Boer, G. Feingold, J. Harrington, M. D. Shupe, and K. Sulia (2011), Resilience of persistent Arctic mixed-phase clouds, *Nat. Geosci.*, *5*(1), 11–17.

Moss, S. J., and D. W. Johnson (1994), Aircraft measurements to validate and improve numerical model parametrisations of ice to water ratios in clouds, *Atmos. Res.*, *34*(1-4), 1–25.

Mossop, S. C., A. Ono, and E. R. Wishart (1970), Ice particles in maritime clouds near Tasmania, *Q. J. R. Meteorol. Soc.*, *96*(409), 487.

Murray, B. J., D. O'Sullivan, J. D. Atkinson, and M. E. Webb (2012), Ice nucleation by particles immersed in supercooled cloud droplets, *Chem. Soc. Rev.*, *41*(19), 6519–6554.

Myers, T. A., and J. R. Norris (2013), Observational evidence that enhanced subsidence reduces subtropical marine boundary layer cloudiness, *J. Clim.*, *26*(19), 7507–7524.

Myers, T. A., and J. R. Norris (2014), On the relationships between subtropical clouds and meteorology in observations and CMIP3 and CMIP5 models, *J. Clim.*, *28*(8), 2945–2967.

Myers, T. A., and J. R. Norris (2016), Reducing the uncertainty in subtropical cloud feedback, *Geophys. Res. Lett.*, *43*, 2144–2148, doi:10.1002/2015GL067416.

Nam, C., S. Bony, J. L. Dufresne, and H. Chepfer (2012), The 'too few, too bright' tropical low-cloud problem in CMIP5 models, *Geophys. Res. Lett.*, *39*, L21801, doi:10.1029/2012GL053421.

Naud, C. M., A. D. Del Genio, and M. Bauer (2006), Observational constraints on the cloud thermodynamic phase in midlatitude storms, *J. Clim.*, *19*(20), 5273–5288.

Norris, J. R., and C. B. Leovy (1994), Interannual Variability in Stratiform Cloudiness and Sea Surface Temperature, *J. Clim.*, *7*, 1915–1925.

O'Dell, C. W., F. J. Wentz, and R. Bennartz (2008), Cloud liquid water path from satellite-based passive microwave observations: A new climatology over the global oceans, *J. Clim.*, *21*(8), 1721–1739.

Platnick, S., M. D. King, S. A. Ackerman, W. P. Menzel, B. A. Baum, J. C. Riedi, and R. A. Frey (2003), The MODIS cloud products: Algorithms and examples from Terra, *IEEE Trans. Geosci. Remote Sens.*, *41*(2), 459–473.

Qu, X., A. Hall, S. Klein, and P. Caldwell (2014), On the spread of changes in marine low cloud cover in climate model simulations of the 21st century, *Clim. Dyn.*, *42*(9-10), 2603–2626.

Qu, X., A. Hall, S. A. Klein, and A. M. DeAngelis (2015), Positive tropical marine low-cloud cover feedback inferred from cloud-controlling factors, *Geophys. Res. Lett.*, *42*, 7767–7775, doi:10.1002/2015GL065627.

Quaas, J. (2012), Evaluating the "critical relative humidity" as a measure of subgrid-scale variability of humidity in general circulation model cloud cover parameterizations using satellite data, *J. Geophys. Res.*, *117*, D09208, doi:10.1029/2012JD017495.

Quinn, P. K., and T. S. Bates (2011), The case against climate regulation via oceanic phytoplankton sulphur emissions, *Nature*, *480*(7375), 51–56.

Rasch, P. J., and J. E. Kristjánsson (1998), A comparison of the CCM3 model climate using diagnosed and predicted condensate parameterizations, *J. Clim.*, *11*(7), 1587–1614.

Storelvmo, T., I. Tan, and A. Korolev (2015), Cloud phase changes induced by CO_2 Warming—A powerful yet poorly constrained cloud-climate feedback, *Curr. Clim. Change Rep.*, *1*, 1–9.

Tan, I., T. Storelvmo, and Y.-S. Choi (2014), Spaceborne lidar observations of the ice-nucleating potential of dust, polluted dust, and smoke aerosols in mixed-phase clouds, *J. Geophys. Res. Atmos.*, *119*, 6653–6665, doi:10.1002/2013JD021333.

Taylor, K. E., M. Crucifix, P. Braconnot, C. D. Hewitt, C. Doutriaux, A. J. Broccoli, J. F. B. Mitchell, and M. J. Webb (2007), Estimating shortwave radiative forcing and response in climate models, *J. Clim.*, *20*(11), 2530–2543.

Trenberth, K. E., and J. T. Fasullo (2010), Simulation of present-day and twenty-first-century energy budgets of the southern oceans, *J. Clim.*, *23*(2), 440–454.

Tsushima, Y., S. Emori, T. Ogura, M. Kimoto, M. J. Webb, K. D. Williams, M. A. Ringer, B. J. Soden, B. Li, and N. Andronova (2006), Importance of the mixed-phase cloud distribution in the control climate for assessing the response of clouds to carbon dioxide increase: A multi-model study, *Clim. Dyn.*, *27*(2-3), 113–126.

Vial, J., J. L. Dufresne, and S. Bony (2013), On the interpretation of inter-model spread in CMIP5 climate sensitivity estimates, *Clim. Dyn.*, *41*(11-12), 3339–3362.

Webb, M. J., F. Lambert, and J. M. Gregory (2013), Origins of differences in climate sensitivity, forcing and feedback in climate models, *Clim. Dyn.*, *40*(3-4), 677–707.

Wilson, T. W., et al. (2015), A marine biogenic source of atmospheric ice-nucleating particles, *Nature*, *525*(7568), 234–238.

Wright, J. S., A. Sobel, and J. Galewsky (2010), Diagnosis of zonal mean relative humidity changes in a warmer climate, *J. Clim.*, *23*(17), 4556–4569.

Zelinka, M. D., S. A. Klein, and D. L. Hartmann (2012), Computing and partitioning cloud feedbacks using cloud property histograms. Part II: Attribution to changes in cloud amount, altitude, and optical depth, *J. Clim.*, *25*(11), 3736–3754.

Zelinka, M. D., S. A. Klein, K. E. Taylor, T. Andrews, M. J. Webb, J. M. Gregory, and P. M. Forster (2013), Contributions of different cloud types to feedbacks and rapid adjustments in CMIP5, *J. Clim.*, *26*(14), 5007–5027.